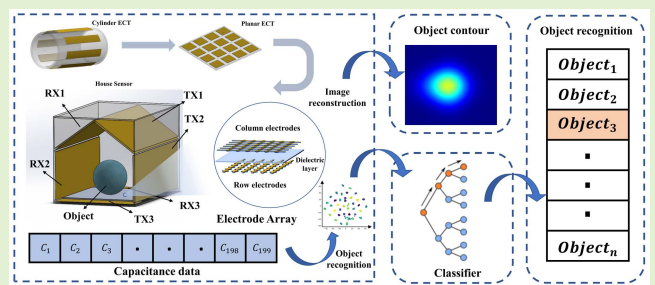


# Electrical Capacitance Tomography Sensor With House Structure for Assisting Recognition of Objects

Zhibin Li<sup>ID</sup>, Graduate Student Member, IEEE, Songhua Xiao, Quan Yue, and Taihong Wang<sup>ID</sup>

**Abstract**—As a fast and non-invasive visualization technology, electrical capacitance tomography(ECT) avoids the problem that camera imaging technology is interfered by light and can't identify material properties. However, the traditional ECT sensor research mainly focused on the image reconstruction of multiphase flow between electrodes, without considering the object recognition performance through the dielectric distribution of the objects. Therefore, we propose a new ECT sensor (called House Sensor) with house-like structure, which is suitable for multi features detection of household objects. We analyze the sensitivity distribution of House Sensor, and use linear back projection(LBP) and Tikhonov regularization for high-speed image reconstruction. 20 objects with different sizes and dielectric constants are visually clustered by t-distributed stochastic neighbor embedding (t-SNE) to verify the feasibility of classification, and the accuracy of Random Forest (RF) is up to 95.3% within 3.5ms. This implies that House Sensor provide a new feasible scheme to assist object recognition under non-vision conditions.

**Index Terms**—Electrical capacitance tomography (ECT), capacitor array, image reconstruction, object recognition, machine learning.



## I. INTRODUCTION

AT PRESENT, the mainstream object recognition scheme is mainly based on the camera image recognition technology, which is called computer vision. This scheme collects image information, analyzes the graphic features of objects, and accurately recognizes complex objects through deep learning. However, such recognition methods usually rely on complex recognition algorithms and require high-performance peripherals and processors. Most importantly, it is highly susceptible to external environmental interference such as blocked objects (known as occlusions) and varying light conditions [1]–[3].

Manuscript received December 16, 2021; accepted January 12, 2022. Date of publication January 14, 2022; date of current version February 28, 2022. This work was supported in part by the Guangdong Major Scientific Research Project (2018KZDXM061) and in part by the China Postdoctoral Science Foundation under Grant 2019M662196. The associate editor coordinating the review of this article and approving it for publication was Prof. M. Jaleel Akhtar. (Zhibin Li and Songhua Xiao contributed equally to this work). (Corresponding author: Taihong Wang.)

The authors are with the Department of Electronic and Electrical Engineering, Southern University of Science and Technology, Shenzhen 518077, China (e-mail: 12032865@mail.sustech.edu.cn; songhuaxiao@foxmail.com; 11930205@mail.sustech.edu.cn; wangth@sustech.edu.cn).

This article has supplementary downloadable material available at <https://doi.org/10.1109/JSEN.2022.3143709>, provided by the authors.

Digital Object Identifier 10.1109/JSEN.2022.3143709

The low efficiency of computer vision in low light environment is mainly solved by multi-sensor fusion, which combines image data with multi-feature sensors information. [4]–[7]. Capacitive sensors have been proposed to identify the shape or material characteristics of objects [8]–[10]. Electrical capacitance tomography (ECT) is an imaging technique, which can measure the external capacitance of an object to obtain its internal dielectric distribution [11], [12]. Compared with other process tomography technologies (such as ultrasonic, optical, X-ray and gamma ray), ECT has the advantages of low cost, fast detection speed, good portability, no radiation and good robustness [9]. This technology has been widely used to measure industrial processes such as two-phase flow [13], fluidized bed [14] and flame development [15].

Most ECT sensor structures are cylindrical structures, and the electrode array is arranged on the cylinder wall, which detects the shape and dielectric distribution of internal objects [12], [16]. This cylindrical structure is mainly used for the detection of multiphase flow substances in the pipeline, which is not suitable to put objects into sensor for object recognition in the context of smart home. Some studies have proposed to design capacitive electrode network on planar fabric [17]. When the target object comes into contact with the electrode network, the object affects the electric field applied by the electrode, and the object can be identified based on the

material and shape of the contact region. Its detection depth is limited, so that its detection ability for high-altitude targets is weak. Recently, a novel 3D image reconstruction method based on planar array ECT is proposed by combining depth estimation and sparse representation [18]. This method reduces the dimension of the unknowns greatly by limiting sparse representation to the plane at the preestimated depth. It demonstrates that the planar array capacitor has high practicability for 3D object contour detection. However, little attention has been paid to the performance of object recognition using ECT sensor to extract the shape and dielectric characteristics of objects.

In this study, we design a new ECT sensor with house-like structure, which is used to recognize objects, which is called House Sensor. The House Sensor is improved on the basis of the traditional cylindrical structure and plane structure, which consists of three pairs of capacitor plates to form a three-dimensional box with a  $14 \times 14$  electrode array on the bottom. Three pairs of capacitor plates detect the mutual capacitance change caused by the objects with different dielectric constant and volume inside the box, which requires a long detection distance and a wide capacitance sensing range. The  $14 \times 14$  electrode array ECT has a staggered rhombic structure, which increases the capacitance between the electrodes far away from each other on different planes and further reduces the interference of measurement signals [19]. For array ECT data, we use linear back projection(LBP) and Tikhonov two most commonly used algorithms to achieve high-speed objects position and contour image reconstruction [20]. Finally, we verify the feasibility of the House Sensor for household objects classification and evaluate its classification performance. This work includes the following contributions:

(1) The improved ECT sensor with house-like structure is used to detect the dielectric distribution of objects, which is better suited to the detection of household objects. We analyze the sensitivity distribution of House Sensor, and use linear back projection (LBP) and Tikhonov regularization for high-speed image reconstruction.

(2) The visual clustering of data is realized by t-distributed stochastic neighbor embedding (t-SNE) to verify the feasibility of House Sensor for object recognition.

(3) The recognition model is established and the algorithm parameters are optimized to evaluate the classification performance of House Sensor. The accuracy of Random Forest (RF) is as high as 96.7%.

(4) Noise sensitivity analysis of object recognition system. Gaussian white noise with a signal-to-noise ratio (SNR) of 70-10dB was added to the test set.

This article aims to propose a new method to assist object recognition under bad visual conditions. The multi capacitance data of the target object is obtained by the House Sensor and used in the classification experiment to further verify the effectiveness of the object recognition method.

## II. SENSOR DESIGN

Rhombic block planar array ECT has been proposed to have good detection effect on objects [17]–[19]. When the object is placed inside the sensor, the object would act as

a dielectric object in the capacitor, and the object would change the dielectric properties and charge distribution in the electric field space. Because the detection depth of planar array electrode is limited, it can only provide the basic contour and position of the target, but it is difficult to obtain more details. Therefore, we designed three pairs of mutual capacitances in space, mainly to detect the global material properties of the object by using the far detection distance. At the same time, the sensor box with house like structure can also better adapt to object recognition under the background of intelligent lockers. In this chapter, we calculate the sensitivity range of the House Sensor through simulation, and then design the hardware of the House Sensor.

### A. Simulation Experiment

In practical experiments, due to the complexity of sensor structure and medium distribution, it is difficult to obtain the accurate solution of sensor sensitive field distribution. The experimental method has high requirements for measurement accuracy and large amount of experiment [21]. Therefore, we choose finite element simulation to calculate the detection depth and sensitivity range of the sensor. In the actual capacitance image reconstruction, the sensitive field matrix is also solved by finite element simulation.

When the boundary conditions of the measurement area are known, the capacitance of the sensor is calculated according to the changes of the objects with different dielectric constants and sizes [22]. The mutual capacitance between two electrodes is derived from given permittivity distribution, according to the Poisson equation:

$$\nabla \cdot \varepsilon(x, y, z) \nabla \phi(x, y, z) = 0 \quad (1)$$

where  $\varepsilon(x, y, z)$  is the permittivity distribution at the coordinate  $(x, y, z)$ , and  $\phi(x, y, z)$  is the electric potential distribution at the coordinate  $(x, y, z)$ . According to the Gauss' flux theorem, without considering the influence of boundary conditions on capacitance value, the expression of capacitance value is as follows [23]:

$$C_{i,j} = \frac{Q}{V} = -\frac{1}{V} \iiint_D \varepsilon_0 \varepsilon(x, y, z) \nabla \phi(x, y, z) dx dy dz \quad (2)$$

where  $C_{i,j}$  is the capacitance between electrodes  $i$  and  $j$ ,  $Q$  is the electrode induced charge,  $V$  is the potential difference between  $i$  and  $j$ ,  $\varepsilon_0$  is the vacuum dielectric constant,  $\varepsilon(x, y, z)$  is the relative dielectric constant at the coordinate  $(x, y, z)$ ,  $\phi(x, y, z)$  is the potential distribution at the coordinate  $(x, y, z)$ ,  $D$  is the test area within the sensor.

According to formula (2), We first solve the electric field changes of a pair of capacitor plates affected by objects. Fig. 1 shows the object proximity capacitance sensing simulation under the condition of a single pair of capacitive plates. The simulation structure of a single pair of capacitive plates is shown in Fig. 1(a). The bottom surface is two electrode plates, and the approaching object is placed directly above the center of the electrode plane. The electrode is defined as a solid copper sheet with the length of 300mm, the width of 200mm, and the thickness of 3mm. The House Sensor is mainly used for the imaging and recognition of household items, and the

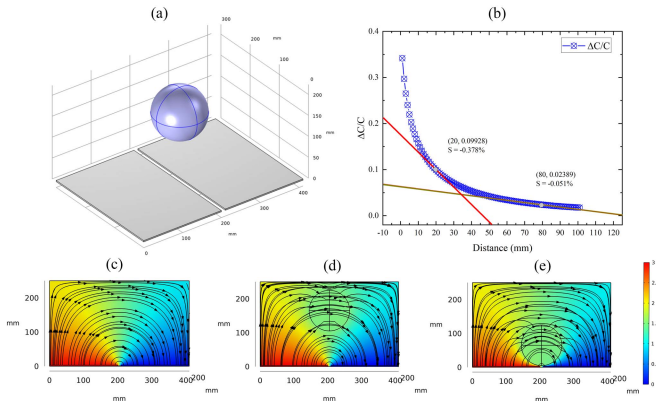


**Fig. 1.** Object proximity sensing simulation under the condition of a single pair of capacitive plates. **(a)** Simulation structure diagram. **(b)** Capacitance changes at different distances. **(c)** Simulation of the electric field when the object is at infinity. **(d)** Simulation of the electric field when the object is 100mm away from the plate. **(e)** Simulation of the electric field when the object is 2mm away from the plate.

dielectric constant of some household items is close to liquid water. In the simulation, we define the approaching object as a sphere with a radius of 60mm, and set the relative dielectric constant of the material to 78, which is close to water.

We apply the 3V voltage between the capacitor plates, which is close to the supply voltage of the measuring circuit. The distance between the surface of the target object and the electrode plane is changed from 100 mm to 1 mm in steps of 1 mm. As shown in Fig. 1(c), 1(d), 1(e), the simulated object gradually approaches the plate from a distance, and the electric field line passing through the space would be offset. The capacitance value between plates at different distances is shown in Fig. 1(b). We can see that as the distance between the sensed object and the electrode becomes shorter, the capacitance value increases. The measurement sensitivity is defined as the slope of the sensor measurement curve, that is, the ratio of the sensor output (capacitance) variation to the experimental physical parameter (distance) variation. When the object is less than 80mm away from the plate, the capacitance change rate is higher than 0.051%. Within 20 mm, the change rate of capacitance with distance increases to more than 0.375%. The results show that the capacitance detection sensitivity increases with the decrease of distance. The closer the target object is to the detection board, the more conducive it is to capacitive object detection. when the target object is 80 mm away from the electrode, the detection sensitivity would be low. This means that the planar mutual capacitance is difficult to detect the part of the object away from the electrode.

The structure of House Sensor is shown in Fig. 2. We design the sensor size according to the size of household items, because we mainly solve the recognition problem of household items (such as apples, mice, tea cups, etc.) in the closed electric field. This structure can also be better adapted to be used in the scene of intelligent lockers for object recognition. The 3D structure design of the House Sensor is shown in Fig. 2 (a). The sensor is a square box with a rhombic roof. The target object is placed in the inner cavity of the box as the dielectric of the electric field. The front view of the sensor is shown in

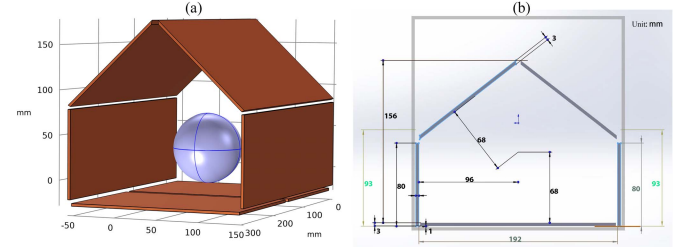


**Fig. 2.** Structural design model of house sensor. **(a)** Three dimensional structure diagram of sensor. **(b)** Front view structure of sensor.

**Fig. 2 (b).** The box is 192 mm wide, 156 mm high, 300 mm deep and the electrode thickness is 3mm. The purpose of our design is to reduce the distance between the object itself and the capacitor plate to less than 100mm, so that the electric field in the space can penetrate the target object.

In the finite element simulation, we change the volume, dielectric constant and position of the target object to solve the change of the electric field in the sensor. We put the spherical object in the center of the capacitance space, with a width of 96mm and a depth of 150mm, and its surface is 5mm away from the base plate. The initial radius of the sphere is 50 mm and the dielectric constant is 78. The electric field simulation inside the sensor is shown in Fig. 3. The distribution of the electric field under the effect of the object in the three-dimensional space of the sensor is shown in Fig. 3(a). The electric field lines of the object position are more intensive because of its larger dielectric constant.

We first simulate the effect of volume change on capacitance. The sphere is placed in the center of the House Sensor, the radius of the sphere is changed from 1mm to 68mm, and the step size is 1mm. As shown in Fig. 3(b), The capacitance between the three pairs of plates increases with the increase of the volume of the object. With the increase of the radius, the sensitivity of the top plate capacitance (Capacitance1) and the side plate capacitance (Capacitance2) increases, and the sensitivity of the bottom plate capacitance (Capacitance3) first increases and then decreases. When the radius is 30mm, the sensitivity of Capacitance1, Capacitance2 and Capacitance3 is respectively 0.021%, 0.039% and 0.125%. When the radius is greater than 50 mm, the sensitivity of the bottom plate capacitor begins to weaken, but the sensitivity of the top plate capacitor increases. This means that when the volume of the object is small, the sensitivity of the base plate capacitor is relatively high, which plays an important role in capacitance detection. When the object volume is large, the sensitivity of the roof capacitor increases, which is helpful to detect large objects.

Then we set the sphere at the center of the sensor, and the relative dielectric constant changes from 1 to 80 in steps of 1. The relationship between capacitance and dielectric constant is shown in Fig. 3c). With the increase of the relative permittivity, the capacitance values of the three capacitors show the upward trend. When the relative permittivity of the object is less than 30, the sensitivity of the top plate capacitance (Capacitance1) is higher than 0.007%, the sensitivity of the side plate (Capacitance2) is higher than 0.004%, and the

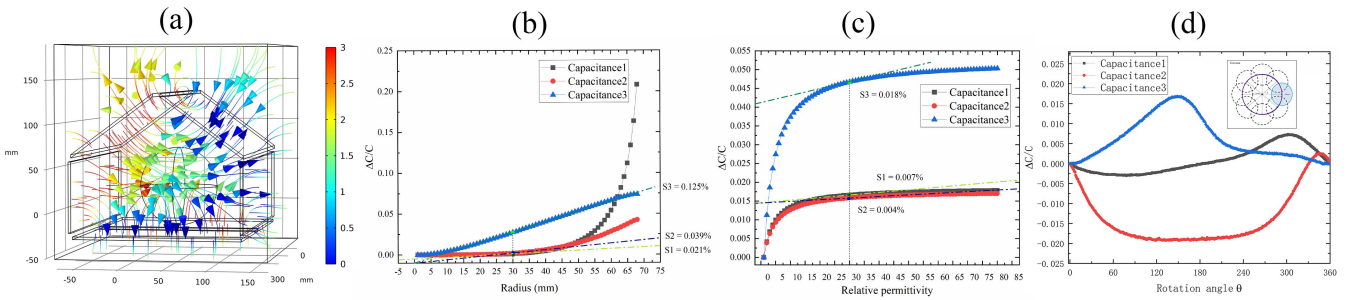


**Fig. 3.** House Sensor electric field simulation. (a) The three-dimensional view of the simulation under the action of an object in the sensor electric field. (b) The capacitance changes with the radius from 0 to 68 mm. (c) The capacitance changes with the dielectric constant from 1 to 80. (d) Variation of capacitance with object position.

sensitivity of the bottom plate capacitance (Capacitance3) is higher than 0.018%. This shows that the capacitive sensor is more inclined to distinguish objects with low relative permittivity.

We set the radius of the object to 30mm and simulate it at different positions on the circumference with a radius of 50mm [24]. The object moves along a circle with an angle step of 1 degree. Therefore, the object position and dielectric distribution can be determined by angle variables  $\theta$ . We express the sampling angle as  $\theta(k)$ ,  $k = 0 \dots 360$ . For each  $\theta(k)$ , the electrode capacitance in the corresponding state is collected. As shown in Fig. 3(d), we can see that the change of the position of the object inside the sensor will cause the capacitance response of different electrodes. This shows that in the process of object recognition, the influence of object placement position on capacitance must be considered.

According to the above simulation experiments, we can use the Shape characteristics and dielectric properties of different objects for image reconstruction and object recognition. Then we design the hardware of House Sensor according to the above structure. Through the actual test of the House Sensor, we further verify the feasibility of its recognition of household objects.

### B. Hardware Design

We design the sensor according to the above simulation structure, and the electrode is made of 3mm thick copper foil. Object recognition depends on the accurate and high-speed acquisition of mutual capacitance between electrodes. Traditional methods such as the measurement circuit of mini-capacitance based on Charging/Discharging Principle have low accuracy and hysteresis [25]. The peripheral electrode adopts the capacitance detection method based on resonance, which has a deep detection range under the certain accuracy [26]. The capacitors (sensor electrodes) to be detected are connected in series into the resonant circuit. By accurately detecting the resonant frequency( $f$ ) of the circuit, the capacitance ( $C_x$ ) of the corresponding electrode can be calculated. The conversion formula between capacitance and frequency is as follows:

$$C_x = \frac{1}{4\pi^2 f^2 L_1} - C_1 \quad (3)$$

where  $L_1$  is the known 18uH inductance,  $C_1$  is the known 33 pF capacitance.  $C_1$  and  $C_x$  are connected to resonant circuit in parallel.

The capacitance acquisition method based on resonant circuit has high robustness for object recognition. It is not easy to be affected by EMI noise, so it has better signal-to-noise ratio (SNR). Secondly, it allows capacitance measurement in a wide range (maximum input capacitance: 250nf) with ultra-high resolution [26]. Three resonant circuits are used to detect the capacitance in three-dimensional space, which is mainly responsible for identifying the material characteristics of the whole object in space.

In recent years, planar ECT array has been applied in object detection, which has high practicability for the detection of contour and dielectric distribution characteristics of complex shape objects [18]. Therefore, the diamond structure is used as a planar array electrode of the underlying array to detect the contour shape of the object. By detecting multiple pairs of capacitor arrays, we can convert them into object position and shape features. The hardware design of the House Sensor is shown in Fig. 4, which show the hardware structure and hardware test results of the sensor. As shown in Fig. 4(a), this is the hardware structure diagram of sensor, and 3 pairs of plates are connected to three groups of resonant circuits respectively. The bottom surface of House Sensor is designed with a double-layer PCB array, which is a  $14 \times 14$  electrode array. The row electrode is the excitation electrode on the lower surface and the column electrode is used as the detection electrode on the upper surface. The working mode of the electrode array is shown in Fig. 4(b). The 3V, 250 kHz square wave is applied on the row electrode as the excitation signal, and the induced voltage signal is detected on the column electrode as the capacitance detection report. In this design, AD7142 is used for electrode array capacitance detection. The chip is integrated with 16Bit C/V converter, phase sensitive demodulation circuit, low-pass filter circuit, phase-shift circuit and signal compensation circuit [27]. The capacitance data of 196 capacitors are detected by scanning 14 rows and 14 columns.

In order to avoid short circuit contact between the bottom electrode and the array electrode, the foam isolation layer is added to the electrode, which is approximately regarded as the air field between the object and the electrode. The process of collecting capacitance data is shown in Fig. 4(c), the peripheral three groups of space capacitors are connected to resonance circuits, and the bottom capacitor array is connected to row and column scanning circuit. In order to prevent crosstalk between capacitor acquisition circuits, we use analog

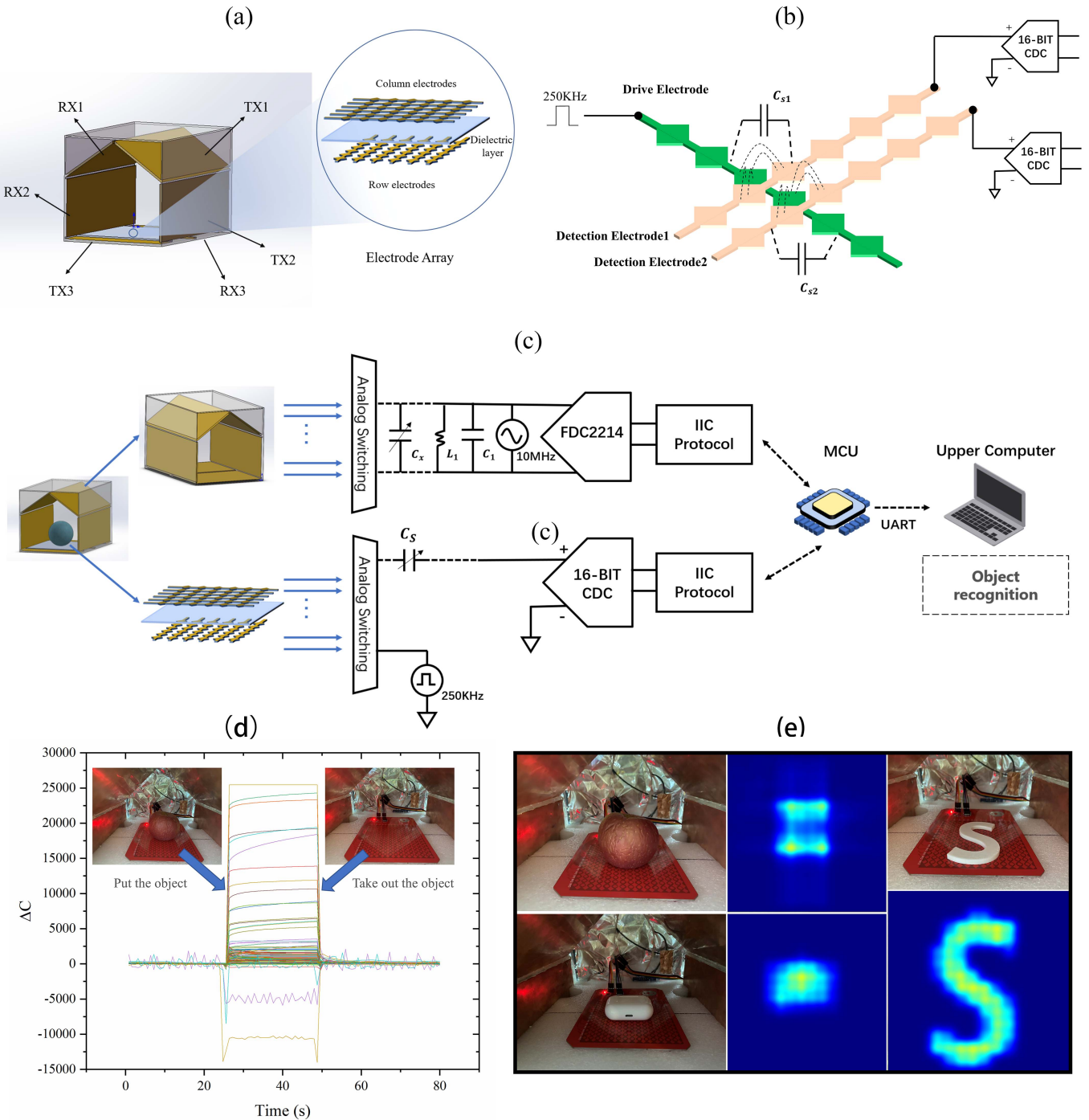


**Fig. 4.** House Sensor hardware design. (a) Sensor hardware structure diagram. (b) Sensor bottom array working principle diagram. (c) Sensor circuit schematic diagram. (d) Sensor data change diagram in the process of putting and taking out objects. (e) Target object imaging diagram.

switch to control the two circuits to scan alternately. On the outer surface of the sensor, we wrap it with aluminum foil and connect it to GND as the shielding layer. The capacitance data of two circuits are collected in one working cycle.

As shown in Fig. 4 (d), we read the capacitance data continuously for 80 s. We put the object at 25 s, and then take it out at 48 s. We can find that 199 channels of capacitance data under the effect of the object have changed significantly. The 196 capacitance data of the bottom array can be used for image reconstruction to observe the shape of the object.

Linear back projection (LBP) is preferred to improve the time efficiency of object image reconstruction [23], [28], [29]. LBP is a fast ECT method by linear mapping from dielectric constant to mutual capacitance. The mapping relation of mutual capacitance is as follows:

$$C = SG \quad (4)$$

where  $C$  is  $m \times 1$  capacitance vector,  $S$  is a  $m \times n$  sensitivity matrix.  $G$  is  $n \times 1$  image vector of dielectric constant, namely the permittivity distribution. In this work,  $m$  is the

number of capacitance data collected by the bottom array,  $m = 196$ .  $n$  is the number of meshes in the reconstructed image,  $n = 100 \times 100$ . The sensitivity matrix  $S$  is calculated using the potential distribution, and the formula is as follows:

$$S_{ij}(x, y, z) = - \iiint \frac{\nabla\phi_i(x, y, z)}{V_i} \frac{\nabla\phi_j(x, y, z)}{V_j} dx dy dz \quad (5)$$

where  $S_{ij}$  is the sensitivity between the  $i$  and  $j$  electrodes regarding the permittivity change in the pixel position of  $v(x, y, z)$ ;  $\nabla\phi_i(x, y, z)$  and  $\nabla\phi_j(x, y, z)$  are the potential distributions when the  $i$ th and  $j$ th electrodes are excited, respectively.  $V_i$  and  $V_j$  represent the excitation voltages applied to  $i$  and  $j$  electrodes. Because the detection depth of planar array electrode is limited, we set the detection height  $z$  of the sensitivity matrix to 5mm. Finally, the sensitivity matrix is normalized for inversion calculation.

According to the above equation, the dielectric distribution image  $G$  of the object is solved as follows:

$$G = S^{-1}C \quad (6)$$

The premise of invertibility of  $S$  is that it is a square matrix and full rank. In fact, the number of capacitance measurements is far less than the number of pixels required, so  $S^{-1}$  may not exist. Therefore, LBP uses the transposition of sensitivity matrix  $S$  to estimate the solution of ill posed equation. The solution formula is as follows:

$$G = S^T C \quad (7)$$

Tikhonov regularization was proposed to solve the ill posed problem accurately and stably, which can transform the process of solving ill posed problem into a universal function optimization process [30], [31]. The dielectric distribution image  $G$  of the object is solved as follows:

$$G = (S^T S + \lambda I)^{-1} S^T C \quad (8)$$

$\lambda I$  is a unit matrix composed of regular parameters, so that matrix  $(S^T S + \lambda I)^{-1}$  always exists. Therefore, the ill conditioned property of ECT solution is effectively weakened. In the actual test, we take  $\lambda$  as 0.01. The capacitance without object is taken as the initial value, and the change value of array capacitance is normalized as the input value  $C$ .

As shown in Fig. 4 (e), We visualized the dielectric constant distribution of the objects. We visualized the contour image of some household objects. The image can well display the dielectric distribution and position characteristics of different objects. Different targets have different imaging shapes and media distribution, which can be used as an important reference standard for object recognition. We can analyze and process the capacitance data, and use it to build the machine learning classification model to evaluate the feasibility of object recognition of House Sensor.

### III. CONSTRUCTION OF CLASSIFICATION MODEL

In this section, the object recognition system based on the House Sensor is proposed. We collect capacitance data, then build machine learning models such as Random Forest (RF)

and Support vector machine (SVM), and simple neural networks such as Multilayer perceptron (MLP) to demonstrate the promising potential of House Sensor for object recognition.

#### A. Dataset Establishment

We build sensor data sets with 20 different household items (such as headphones, bank cards, fruits, etc.). The household items used for the test are shown in Fig. 5 (a), including food, tools and daily necessities. Objects with different geometric and material properties are selected in the dataset [32], and their main body is composed of non-metal. We also select some objects with similar geometry but different material properties to highlight the subtle differences that the sensor can recognize. For example, the same shape of campus card and bus card; Under the same cup condition, the empty cup and the water cup are the same; Oranges and apples of similar size, wet and dry tissue, etc. At the same time, the apple and orange categories contain two individuals with different shapes.

In order to avoid the decline of classification accuracy caused by objects in different positions and postures, we need to increase the diversity of data sets. We selected six laboratory students as experimenters, who randomly placed the target object on the bottom plate inside the sensor. The object is placed arbitrarily in the way the experimenter is used to. For each experimenter, we collect 20 sets of data for each sample. This ensures that the dataset contains as many general position and pose features of the object as possible.

We use t-distributed stochastic neighbor embedding (t-SNE) to verify that capacitance data features are effective for item classification. The t-SNE is a common feature visualization method, which reduces the dimension of high-dimensional data features to two-dimensional or three-dimensional to establish feature map [33]. In the visualization phase, more separated functions are better classified. As shown in Fig. 5 (a), we use t-SNE to reduce the feature dimension of 20 categories of items and map them into a two-dimensional feature map. We can clearly see the separation of features between categories. This emphasizes that House Sensor is feasible for home objects classification. We specially select items with similar shape for feature comparison. As shown in Fig. 5 (c), (d), We use t-SNE to reduce the feature dimension of apple and orange, traffic card and student card, and map the features to the three-dimensional feature map. It can be seen that there are still feature differences between objects with similar morphology, which would be an important basis for establishing classification model. We would further use the 199 channel capacitance data of the above 20 categories as the training set and test set to establish the object classification model.

#### B. Data Processing

Before collecting sensor data for model building, we subtract the background noise from the original sensor data. The background noise data is the average value  $C_f^{i,average}$  of 199 channels readings with a window of 20 when there is no object placed. After initialization, MCU read the sensor capacitance  $C_f^{i,j}$  continuously. ( $i$  is the serial number of capacitance channel, which ranges from 0 to 198,  $j$  is the

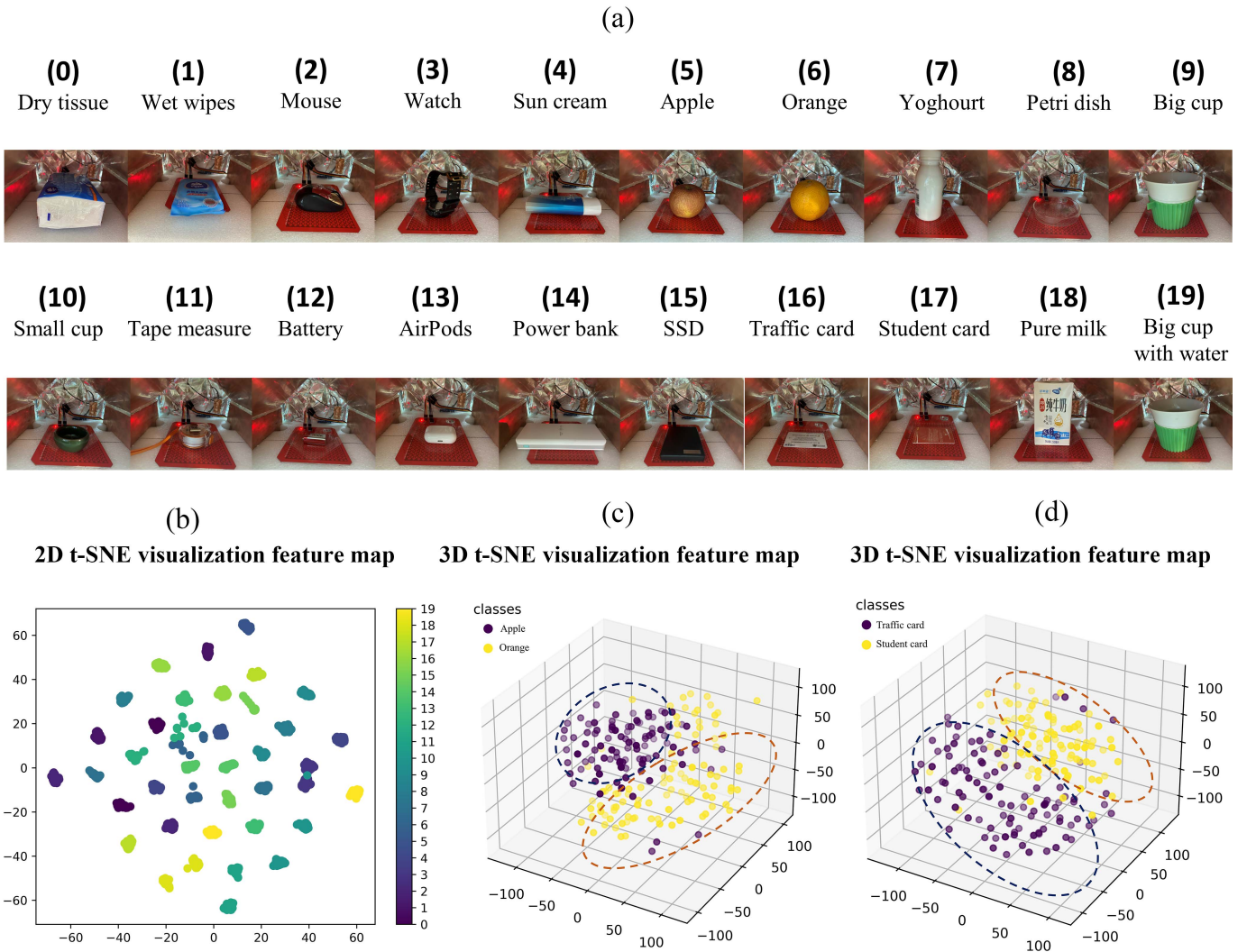


**Fig. 5.** Dataset description. (a) Schematic diagram of 20 classification experimental objects. (b) 2D t-SNE visualization feature map of 20 classification experimental objects. (c) 3D t-SNE visualization feature map of apple and orange. (d) 3D t-SNE visualization feature map of traffic card and student card.

time serial number of capacitance acquisition). Then subtract the average value from the capacitance value to calculate the capacitance change  $\Delta C_f^{i,j}$ .

$$\Delta C_f^{i,j} = C_f^{i,j} - C_f^{i,\text{average}} \quad (9)$$

$\Delta C_f^{i,j}$  is used as the characteristic value of recognition. The items described in the previous section as shown in Fig. 5 (a) are used as the data set of the model. The dataset contains object features in different positions and poses. Then the data is standardized to get  $x_{i,j}$ .

$$x_{i,j} = \frac{\Delta C_f^{i,j} - \mu^i}{\sigma^i} \quad (10)$$

where  $\mu^i$  is the mean value of  $\Delta C_f^{i,j}$  and  $\sigma^i$  is the standard deviation of  $\Delta C_f^{i,j}$ .  $x_{i,j}$  is the characteristic value of object classification. It is used as the input of classification model. We don't need feature extraction or filtering for sensor data any more, because this study aims to show the performance of

the original capacitance data of the sensor when recognizing objects.

### C. Machine Learning

We use the capacitance data of the above objects to build a machine learning classification model. Random forest is the main recognition algorithm for training and testing, which has high efficiency and low requirement on hardware. It is suitable to be transplanted to the off-line embedded platform for real-time object recognition to meet the application in smart home environment.

Random forest (RF) [34] is an improved classifier for Bootstrap aggregation (Bagging) algorithm in parallel integration learning. Its main feature is to introduce random attribute selection in the training process of multiple decision trees. The selection of random attributes in Random Forest is mainly used in two aspects. Firstly, in the data set, the training data used in the decision tree construction is generated by random extraction with the return of the original data set. Secondly, on the feature set, the feature of decision tree is randomly

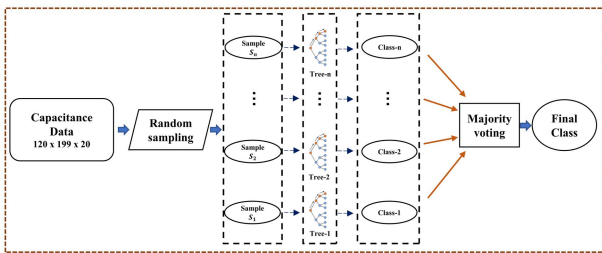


Fig. 6. Random forest flow chart.

extracted from the original feature set. Such random selection makes classification model not easy to fit, and improves the generalization ability of the model. This also meets the requirement that House Sensor can get high accuracy without feature screening, and has good robustness to the features.

The flow chart of Random Forest algorithm is shown in Fig. 6. We take the capacitance data of multi-channel sensor as the model input. The training data includes capacitance data of 199 channels of 20 objects. And construct  $n$  decision trees to form random forest. The training process of the model is as follows:

(1) Extract  $n$  times from the data set to form  $n$  different training sets as the input of the weak classifier;

(2)  $n$  different training sets are used to train different decision tree models;

(3) Gini coefficient is used to select the optimal partition attribute for node splitting of decision tree. The Gini coefficient is  $I_G$ :

$$I_G = \sum_{i=1}^m f_i (1 - f_i) \quad (11)$$

where  $f_i$  is the proportion of class  $i$  samples in the current sample set,  $m$  is the number of randomly selected features, and  $m$  is less than the total number of classification features. To find the segmentation points of the feature when  $I_G$  gets the minimum value, and divide the data set into two subsets;

(4) Cycle through the above steps (2), (3) until all the training samples of the node belong to the same class or reach the maximum depth of the tree;

(5) A total of  $n$  data sets were extracted to construct  $n$  decision trees, which were combined to form a random forest model. Multiple decision trees vote to determine the final classification result.

#### IV. RESULT AND DISCUSSION

We use the above House Sensor data to train and test the random forest model, and cross validation method to test the model. The data set is divided into 10 subsets, including 8 subsets as training set and 2 subsets as test set. We take *Accuracy* as an important index to judge the performance of the classifier. In addition, *Precision*, *Recall* and *F1\_score* are used as reference indexes in the model comparison stage. The formula is as follows:

$$\text{Accuracy} = \frac{TP + TN}{TP + FP + FN + TN} \times 100\% \quad (12)$$

$$\text{Precision} = \frac{TP}{TP + FP} \times 100\% \quad (13)$$

$$\text{Recall} = \frac{TP}{TP + FN} \times 100\% \quad (14)$$

$$\text{F1\_score} = \frac{2 \times TP}{2 \times TP + FP + FN} \times 100\% \quad (15)$$

where:  $TP$  is true positive, indicating that the actual category is positive and the algorithm output category is also positive;  $FP$  is false positive, indicating that the actual category is negative and the sample output category is positive;  $TN$  is false negative, which means that the actual category is negative, and the output class of algorithm is negative;  $FN$  is false negative, indicating that the actual category is positive and the algorithm output category is negative.

According to formula (11), We take the Gini coefficient as the measure of model impurity. In Random Forest model training, the number of decision trees  $n$  has the important influence on the final classification results. The training test results show that when  $n$  is small, the classification error of Random Forest would be large; When  $n$  increases gradually, the accuracy of Random Forest classification would be significantly improved, but it would eventually become stable, or even decline. But when the  $n$  is larger, the memory would be larger, and the time of training and prediction would increase accordingly, so we should select the appropriate number of decision trees as much as possible within the acceptable range. Parameter *Max\_features* represents the maximum number of features considered when constructing the optimal model of decision tree.  $N$  is the total number of features in the dataset. We set the model parameter *Max\_features* as  $N$ ,  $\log_2(N)$  and  $\sqrt{N}$  for optimization experiments. The parameter *Max\_depth* represents the maximum depth of the decision tree. When there are many samples and features of the model, the selection of *Max\_depth* would optimize the complexity of the model.

We optimize the number of decision trees  $n$  and the maximum number of features *Max\_features* for model classification experiments. The training chart is shown in Fig. 7 (a), it can be seen that when the number of decision trees is more than 30, the accuracy of the model has tended to converge. In this work, the number of decision trees of 30 is more moderate, and the classification accuracy is higher than 94%. When *Max\_features* =  $\sqrt{N}$ , the accuracy of the model is better. In this work, we set the maximum number of features as  $\sqrt{N}$ . As shown in Fig. 7 (b), when the maximum depth of the model is greater than 15, the accuracy rate converges. We set the model parameter *Max\_depth* as 15.

In order to test the robustness of the House Sensor, we added 70-10dB Gaussian white noise in the collected test data set to simulate the actual noise of EIT hardware system [35]. We first calculate the noise power  $P_{\text{noise}}$  from the test data:

$$P_{\text{noise}} = \frac{P_{\text{signal}}}{10^{\frac{\text{SNR}}{10}}} \quad (16)$$

where SNR is the signal-to-noise ratio coefficient,  $P_{\text{signal}}$  is the power of the original signal.

$$P_{\text{signal}} = \frac{1}{n} \sum_{k=1}^n C_k^2 \quad (17)$$

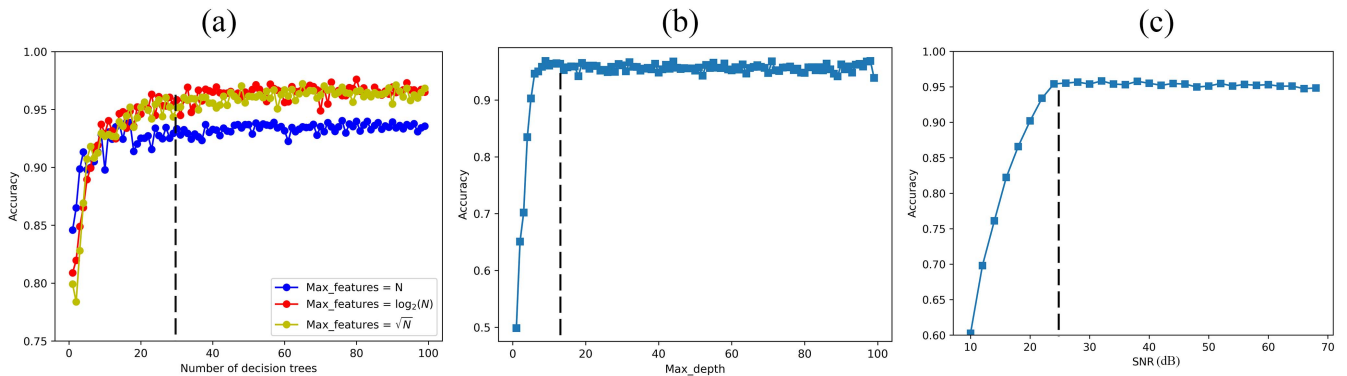


**Fig. 7.** Model optimization **(a)** The classification accuracy varies with the number of decision trees and maximum number of features. **(b)** The classification accuracy varies with the maximum depth of the model. **(c)** Model recognition accuracy under different SNR.

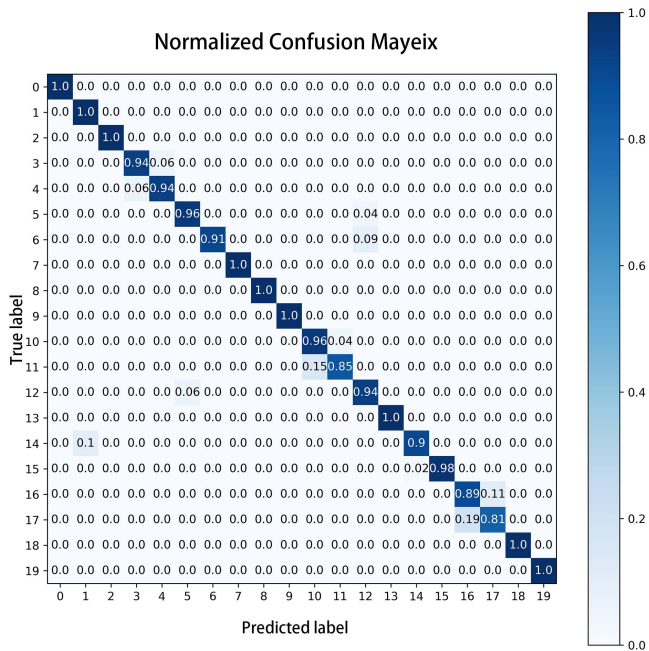


**Fig. 8.** The confusion matrix of classification results.

where  $C_k$  is the discrete capacitance data sequence. After obtaining the power of noise, we form a noise sequence with power determined standard Gaussian distribution (mean value is 0 and standard deviation is 1). Finally, the noise sequence is added to the original test signal to obtain the test signal. As shown in Fig. 7 (c), when the noise gradually increases, the object recognition accuracy decreases. Especially when SNR is less than 20dB, the recognition rate decreases significantly. However, when SNR is greater than 25dB, the system has high accuracy, which is greater than 95%. This proved that the system has a certain ability to resist noise, which is very important for object recognition in real environment.

We trained the classifier of 20 household items, and the final average accuracy of the RF model is 95.3%. The confusion matrix of classification results is shown in Fig. 8. The results of confusion matrix show that the recognition accuracy of

each category is more than 80%. The recognition accuracy of label 17 is the lowest, which is 81 %. The label 17 is the student card, which is easily confused with the traffic card of label 16. Because the size of the two cards is small and the appearance is the same, the sensor can only distinguish the internal magnetic stripe through weak difference. In the simulation, we can find that the detection ability of top plate and side plate to small objects is weak. Therefore, our sensor has low sensitivity to small objects, and it is challenging to accurately identify small objects.

It is gratifying that House Sensor has achieved excellent results in the recognition of large volume objects with different dielectric properties. It can distinguish different kinds of fruits with similar appearance (for example, label 5 and label 6) and empty cup and same cup with the water (for example, label 9 and label 19), and the accuracy exceeds 90%. The water content of the object has a great influence on the capacitance detection, which would be used as an important standard to judge whether the container contains water. The sensor can well recognize objects with different sizes and shapes. This fully confirms the feasibility of House Sensor in recognizing objects with different dielectric properties and appearance.

In order to further illustrate the effectiveness of House Sensor for object recognition, we compare the RF classifier with the traditional machine learning method SVM classifier [36], [37] and the simple artificial neural network Multilayer perceptron (MLP) [38], [39]. SVM classifiers are built by using the one vs rest framework, and the penalty coefficient C is set to 1, and the kernel function coefficient is selected as RBF. MLP includes input layer, hidden layer and output layer, and all layers are connected by full connection. We set the number of hidden layers in the middle to 1, the number of neurons as 64, and the excitation function as 'relu'. The number of neurons in input layer is 199, and the activation function is 'relu'. The number of neurons in the output layer is 20, and the activation function is 'softmax'. The comparison of test results is shown in Table I.

The experimental results in Table I show that the recognition accuracy of the three simple classification models is above 94%. MLP has a relatively high recognition rate, but it takes a long time to recognize, and the classification model is more

**TABLE I**  
COMPARISON OF CLASSIFIER RESULT

Classifier	Precision	Recall	F1-score	Accuracy	Time (S)
RF	95.5 %	95.3%	95.3%	95.3%	0.0035
SVM	94.8%	94.6%	94.6%	94.6%	0.0020
MLP	97.1%	96.9%	96.9%	96.9%	0.1211

Note: Time is expressed as the time required for the classifier to classify a set of data.

complex than Random Forest. The difference of recognition accuracy among the three methods is small, and SVM takes the shortest time. However, the training process of support vector machine is usually time-consuming, because when dealing with multi classification problems, we need to use the “one vs rest” framework, which requires a large amount of memory. In comparison, RF can quickly classify House Sensor data with less computation.

This means that House Sensor can play a good auxiliary role for object recognition under non-visual conditions, especially used as smart lockers in smart homes and smart stores. It is mainly used for the auxiliary identification of the items inside the box in the environment of no light or weak light, and can distinguish the morphology and material properties. However, there are still some challenges in the object recognition application of House Sensor. In some extreme positions or facing objects with special shapes, the recognition accuracy will decrease significantly, so it is necessary to ensure the diversity of the training set. Building a data set requires repeatedly putting a large number of samples randomly into the sensor, which is a very cumbersome process. At the same time, the system still has the challenge to multi-object simultaneous detection and recognition, which is an arduous task. For more real applications, further testing of larger data sets and additional research on advanced learning algorithms are still needed.

## V. CONCLUSION

In this study, we reported a new ECT sensor with a house-like structure for sensing dielectric properties of objects. By improving the detection of ECT sensor for object shape and dielectric distribution, the object can be quickly imaged and identified. We used this sensor to build machine learning classifiers, which recognized 20 different household items with the accuracy of more than 95.3%. Our work illustrated that this was a new method to assist object recognition under non-visual conditions. We demonstrated the application scenario of household items recognition, and thought that House Sensor would be used as an object recognition auxiliary tool, which was an important step to realize the new interactive smart home and smart shop.

## ACKNOWLEDGMENT

The authors would like to thank all the members of Intelligent Sensor Laboratory, South University of Science and Technology for their help during experiments.

## REFERENCES

- [1] K. E. A. van de Sande, T. Gevers, and C. G. M. Snoek, “Evaluating color descriptors for object and scene recognition,” *IEEE Trans. Pattern Anal. Mach. Intell.*, vol. 32, no. 9, pp. 1582–1596, Sep. 2010.
- [2] X. Tan and W. Triggs, “Enhanced local texture feature sets for face recognition under difficult lighting conditions,” *IEEE Trans. Image Process.*, vol. 19, no. 6, pp. 1635–1650, Feb. 2010.
- [3] K. G. Lore, A. Akintayo, and S. Sarkar, “LLNet: A deep autoencoder approach to natural low-light image enhancement,” *Pattern Recognit.*, vol. 61, pp. 650–662, Jan. 2017.
- [4] C. Chen, R. Jafari, and N. Kehtarnavaz, “A survey of depth and inertial sensor fusion for human action recognition,” *Multimedia Tools Appl.*, vol. 76, no. 3, pp. 4405–4425, 2017.
- [5] N. Dawar, S. Ostadabbas, and N. Kehtarnavaz, “Data augmentation in deep learning-based fusion of depth and inertial sensing for action recognition,” *IEEE Sensors Lett.*, vol. 3, no. 1, pp. 1–4, Jan. 2019.
- [6] K. Liu, C. Chen, R. Jafari, and N. Kehtarnavaz, “Fusion of inertial and depth sensor data for robust hand gesture recognition,” *IEEE Sensors J.*, vol. 14, no. 6, pp. 1898–1903, Jun. 2014.
- [7] W. Huang, L. Zhang, W. Gao, F. Min, and J. He, “Shallow convolutional neural networks for human activity recognition using wearable sensors,” *IEEE Trans. Instrum. Meas.*, vol. 70, pp. 1–11, 2021.
- [8] Y. Guo, X. Wang, S. Wang, K. Hu, and W. Wang, “Identification method of coal and coal gangue based on dielectric characteristics,” *IEEE Access*, vol. 9, pp. 9845–9854, 2021.
- [9] Y. Ye, C. Zhang, C. He, X. Wang, J. Huang, and J. Deng, “A review on applications of capacitive displacement sensing for capacitive proximity sensor,” *IEEE Access*, vol. 8, pp. 45325–45342, 2020.
- [10] W. Tian, P. Suo, D. Liu, S. Sun, J. Sun, and L. Xu, “Simultaneous shape and permittivity reconstruction in ECT with sparse representation: Two-phase distribution imaging,” *IEEE Trans. Instrum. Meas.*, vol. 70, pp. 1–14, 2020.
- [11] D. O. Acero, S. M. Chowdhury, Q. M. Marashdeh, and F. L. Teixeira, “Efficient and flexible sensitivity matrix computation for adaptive electrical capacitance volume tomography,” *IEEE Trans. Instrum. Meas.*, vol. 70, pp. 1–10, 2020.
- [12] S. Sun *et al.*, “Sensitivity guided image fusion for electrical capacitance tomography,” *IEEE Trans. Instrum. Meas.*, vol. 70, pp. 1–12, 2020.
- [13] S. Sun *et al.*, “Real-time imaging and holdup measurement of carbon dioxide under CCS conditions using electrical capacitance tomography,” *IEEE Sensors J.*, vol. 18, no. 18, pp. 7551–7559, Sep. 2018.
- [14] M. Mao, J. Ye, H. Wang, J. Zhang, and W. Yang, “Evaluation of excitation strategy with multi-plane electrical capacitance tomography sensor,” *Meas. Sci. Technol.*, vol. 27, no. 11, Nov. 2016, Art. no. 114008.
- [15] D. Hu, Z. Cao, S. Sun, J. Sun, and L. Xu, “Dual-modality electrical tomography for flame monitoring,” *IEEE Sensors J.*, vol. 18, no. 21, pp. 8847–8854, Nov. 2018.
- [16] M. Meribout and I. M. Saied, “Real-time two-dimensional imaging of solid contaminants in gas pipelines using an electrical capacitance tomography system,” *IEEE Trans. Ind. Electron.*, vol. 64, no. 5, pp. 3989–3996, May 2017.
- [17] T.-Y. Wu, L. Tan, Y. Zhang, T. Seyed, and X.-D. Yang, “Capacitivo: Contact-based object recognition on interactive fabrics using capacitive sensing,” in *Proc. 33rd Annu. ACM Symp. User Interface Softw. Technol.*, Oct. 2020, pp. 649–661.
- [18] P. Suo, J. Sun, W. Tian, S. Sun, and L. Xu, “3-D image reconstruction in planar array ECT by combining depth estimation and sparse representation,” *IEEE Trans. Instrum. Meas.*, vol. 70, pp. 1–9, 2021.
- [19] J. Shen, S. Meng, J. Wang, W. Yang, and M. Ye, “Study on the shape of staggered electrodes for 3-D electrical capacitance tomography sensors,” *IEEE Trans. Instrum. Meas.*, vol. 70, pp. 1–10, 2021.
- [20] H. Zhu, J. Sun, J. Long, W. Tian, S. Sun, and L. Xu, “Deep image refinement method by hybrid training with images of varied quality in electrical capacitance tomography,” *IEEE Sensors J.*, vol. 21, no. 5, pp. 6342–6355, Mar. 2021.
- [21] A. M. Olmos, J. A. Primicia, and J. F. Marron, “Simulation design of electrical capacitance tomography sensors,” *IET Sci., Meas. Technol.*, vol. 1, no. 4, pp. 216–223, 2007.
- [22] T. Murai and Y. Kagawa, “Electrical impedance computed tomography based on a finite element model,” *IEEE Trans. Biomed. Eng.*, vol. BME-32, no. 3, pp. 177–184, Mar. 1985.
- [23] C. G. Xie *et al.*, “Electrical capacitance tomography for flow imaging: System model for development of image reconstruction algorithms and design of primary sensors,” *IEE Proc. G, Circuits, Devices Syst.*, vol. 139, no. 1, pp. 89–98, Feb. 1992.

- [24] S. Ren, R. Guan, G. Liang, and F. Dong, "RCRC: A deep neural network for dynamic image reconstruction of electrical impedance tomography," *IEEE Trans. Instrum. Meas.*, vol. 70, pp. 1–11, 2021.
- [25] K. Thiagarajan, G. K. Rajini, and D. Maji, "Flexible, highly sensitive paper-based screen printed MWCNT/PDMS composite breath sensor for human respiration monitoring," *IEEE Sensors J.*, vol. 21, no. 13, pp. 13985–13995, Jul. 2021.
- [26] (Mar. 28, 2021). *Capacitive Proximity Sensing Using FDC2xIy*. [Online]. Available: <https://www.ti.com/product/cn/FDC2214>
- [27] (Mar. 2021). *AD7142 Data Sheet*. [Online]. Available: <https://www.analog.com/en/products/ad7142.html>
- [28] S. M. Huang, A. B. Plaskowski, C. G. Xie, and M. S. Beck, "Tomographic imaging of two-component flow using capacitance sensors," *J. Phys. E, Sci. Instrum.*, vol. 22, no. 3, p. 173, 1989.
- [29] H. Herdian, I. Muttaqin, A. Saputra, A. Yusuf, W. Widada, and W. P. Taruno, "Hardware implementation of linear back-projection algorithm for capacitance tomography," in *Proc. 4th Int. Conf. Instrum., Commun., Inf. Technol., Biomed. Eng. (ICICI-BME)*, Nov. 2015, pp. 124–129.
- [30] A. N. Tikhonov and V. Y. Arsenin, *Solutions of Ill-Posed Problems*, vol. 1, no. 30, New York, NY, USA, 1977, p. 487.
- [31] M. Vauhkonen, D. Vadász, P. A. Karjalainen, E. Somersalo, and J. P. Kaipio, "Tikhonov regularization and prior information in electrical impedance tomography," *IEEE Trans. Med. Imag.*, vol. 17, no. 2, pp. 285–293, Apr. 1998.
- [32] G. Li, S. Liu, L. Wang, and R. Zhu, "Skin-inspired quadruple tactile sensors integrated on a robot hand enable object recognition," *Sci. Robot.*, vol. 5, no. 49, Dec. 2020, Art. no. eabc8134.
- [33] L. Van der Maaten and G. Hinton, "Visualizing data using t-SNE," *J. Mach. Learn. Res.*, vol. 9, no. 11, pp. 2579–2605, 2008.
- [34] L. Breiman, "Random forests," *Mach. Learn.*, vol. 45, no. 1, pp. 5–32, 2001.
- [35] Y. Y. Guo, X. Y. Chen, and Y. Z. Yang, "A low noise power design for electrical impedance tomography system," *Appl. Mech. Mater.*, vols. 670–671, pp. 1159–1162, Oct. 2014.
- [36] J. A. K. Suykens and J. Vandewalle, "Least squares support vector machine classifiers," *Neural Process. Lett.*, vol. 9, no. 3, pp. 293–300, Jun. 1999.
- [37] D. J. Pasadas, P. Baskaran, H. G. Ramos, and A. L. Ribeiro, "Detection and classification of defects using ECT and multi-level SVM model," *IEEE Sensors J.*, vol. 20, no. 5, pp. 2329–2338, Mar. 2020.
- [38] G. Singh and M. Sachan, "Multi-layer perceptron (MLP) neural network technique for offline handwritten gurmukhi character recognition," in *Proc. IEEE Int. Conf. Comput. Intell. Comput. Res.*, Dec. 2014, pp. 1–5.
- [39] J. Tang, C. Deng, and G.-B. Huang, "Extreme learning machine for multilayer perceptron," *IEEE Trans. Neural Netw. Learn. Syst.*, vol. 27, no. 4, pp. 809–821, Apr. 2015.



**Zhibin Li** (Graduate Student Member, IEEE) is pursuing the Graduate degree with the Department of Electronic and Electrical Engineering, Southern University of Science and Technology, China. His research focuses are intelligent sensor for human-computer interaction and health monitoring.

He won the Third Prize for 2018 National Undergraduate Electronic Design Competition (TI Cup). In 2018, he was designated as Meritorious Winner at Interdisciplinary Contest in Modeling. He won the First Prize for 2019 National Undergraduate Electronic Design Competition (TI Cup). In 2020, he won the Second Prize for National Post-Graduate Mathematical Contest in Modeling.



**Songhua Xiao** received the bachelor's degree from the Department of Automation, Xiamen University, in 2012, and the Ph.D. degree from the Pen-Tung Sah Institute of Micro-Nano Science and Technology, Xiamen University, in 2019. He is currently a Postdoctoral Researcher with the Department of Electronic and Electrical Engineering, Southern University of Science and Technology, China. His current research interests involve the development and application of capacitance sensing devices.



**Quan Yue** is pursuing the Graduate degree with the Department of Electronic and Electrical Engineering, Southern University of Science and Technology, China. His research focuses are intelligent sensor and manufacturing of smart biomaterials.



**Taihong Wang** received the Ph.D. degree from the Institute of Physics, Chinese Academy of Sciences, China, in 1993. He is currently a Chair Professor with the Southern University of Science and Technology, Shenzhen, China. His area of expertises are sensing and intelligent perception.

He was selected as the "Highly Cited Researchers" of Clarivate in 2018. In 1998, he was selected into the "Hundred Talents Program" of the Chinese Academy of Sciences. In 1999, he was funded by the National Science Fund for Distinguished Young Scholars. In 2005, he was hired as the Yangtze River Scholar Professor. In 2006, he was awarded Special Subsidies of the Government of the State Council. In 2007, he was hired as a Chief Scientist of National 973 Project. In 2008, he won the First Prize of Natural Science Award of Ministry of Education.